J Nanopart Res (2012) 14:1098
DOI 10.1007/s11051-012-1098-8

RESEARCH PAPER

Films of covalently bonded gold nanoparticles synthesized by a sol–gel process

Ignacio E. dell'Erba · Cristina E. Hoppe · Roberto J. J. Williams

Received: 23 September 2011 / Accepted: 24 July 2012 / Published online: 3 August 2012

Abstract Gold nanoparticles (NPs) with a size close to 1.5 nm, coated with organic ligands bearing $Si(OEt)_3$ groups, were synthesized and used to obtain self-standing films by a sol–gel process catalyzed by formic acid. Using FESEM images, FTIR, and UV–visible spectra, it was observed that very small gold NPs self-assembled by Si–O–Si covalent bonds forming crosslinked clusters with sizes up to about 50 nm in which NPs preserve their individuality. The possibility of fixing very small gold NPs in a crosslinked film opens a variety of potential applications based on the specific properties of small-size particles. As an example, we illustrated the way in which one can take advantage of the low melting temperature of these NPs to generate tiny gold crystals partially embedded at the surface, a process that might be used for the development of catalysts or sensors. Besides, the shift and change in the intensity of the plasmon band produced by heating to 100 °C may be employed to develop an irreversible sensor of undesirable temperature excursions during the life-time of a specific product.

Keywords Crosslinking · Films · Gold nanoparticles · Self-assembly · Sol–gel

I. E. dell'Erba · C. E. Hoppe (✉) · R. J. J. Williams
Institute of Materials Science and Technology (INTEMA), University of Mar del Plata and National Research Council (CONICET), Av. J. B. Justo 4302, 7600 Mar del Plata, Argentina
e-mail: hoppe@fi.mdp.edu.ar

Introduction

Films formed by the self-assembly of metal nanoparticles (NPs) have deserved widespread interest due to their potential applications in several fields such as nanoelectronics, plasmonics, and sensors (Hu et al. 2005; Ghosh and Pal 2007; Kinge et al. 2008; Ofir et al. 2008; Prasad et al. 2008; Ko et al. 2008; Xiong and Busnaina 2008; Lim and Zhong 2009; Wang et al. 2010). In particular, the collective surface plasmon band of gold NP films and their use as substrates for surface-enhanced vibrational spectroscopy has been analyzed in recent articles and reviews (Ko et al. 2008; Yamada and Nishihara 2004; Fan and Brolo 2008; Baia et al. 2009; Rajesh et al. 2010).

Different methods of NPs assembly during film formation have been explored. These include the simple drying-mediated assembly and the chemically assisted assembly exploiting covalent and non-covalent interactions of the organic ligands stabilizing the metal NPs, with a large variety of crosslinkers and chemical templates (Huo and Worden 2007; Kinge et al. 2008; Selvam et al. 2011). In most of these studies, the starting NPs had dimensions in the range of several nanometers to tenths of nanometers. The self-assembly of small metallic NPs with sizes in the range of 1–2 nm has received considerably less attention possibly due to the intrinsic instability of NPs of this size to most processing conditions. However, films formed by the self-assembly of small metallic NPs might generate new applications based

on their specific properties. For example, the low melting temperature of small NPs might be used to generate small metallic crystals by a coalescence process induced by heating to low temperatures. This might be useful for applications in catalysis and sensors.

In this study, we report the synthesis of 1.5-nm gold NPs functionalized with triethoxysilane $Si(OEt)_3$ groups and their crosslinking by a sol–gel process at room temperature leading to self-standing films. The synthesis of gold NPs functionalized with silanol or alkoxysilane groups has been described in the literature (Liz-Marzán et al. 1996; Buining et al. 1997; Schulzendorf et al. 2011). They were used as precursors of either gold–silica core–shell NPs where the silica acts as an optically transparent and chemically inert coating stabilizing the gold core (Liz-Marzán et al. 1996; Schulzendorf et al. 2011) or of amine-functionalized NPs by reaction with (3-aminopropyl)triethoxysilane (Buining et al. 1997).

In our case, crosslinked films containing 1.5-nm gold NPs were produced by the hydrolysis and condensation of the Si(OEt) groups in dimethylformamide (DMF), adding an aqueous solution of formic acid. This acid participates in the reaction both as a catalyst and as a reactant forming Si(OOCH) intermediates that generate Si–O–Si bonds by reaction with Si(OEt) groups (Sharp 1994; Eisenberg et al. 2002). However, as most acid catalysts, it promotes a fast hydrolysis of Si(OEt) to SiOH groups followed by a slow polycondensation process. In this way, the self-assembly of gold NPs took place at a very slow rate both by covalent bonding and by solvent evaporation at room temperature. The nanostructuration of the resulting film was analyzed as well as the effect of temperature on the evolution of its structure.

Experimental

Materials

Tetraoctylammonium bromide (TOAB, Aldrich), 6-mercaptohexanol (MCH, 97 %, Aldrich), chloroauric acid ($HAuCl_4$, 99.9 %, Aldrich), $NaBH_4$ (>96 %, Fluka), and (3-isocyanatepropyl)triethoxysilane (IPTES >95 %, Fluka) were used as received.

Synthesis of gold NPs

Synthesis of OH-functionalized gold NPs

These NPs were prepared by a previously described procedure (Tan et al. 2006) leading to NPs with an average size close to 1.5 nm. In brief, aqueous $HAuCl_4$ (10 mL, 0.015 M) was mixed with 20 mL toluene and 0.25 g TOAB. This two-phase mixture was shaken for 30 min, thus transferring gold from the aqueous to the organic phase. Then, 24 mg MCH were added (molar ratio S/Au = 1.2) and the mixture was stirred for another 20 min. Finally, 2 mL of a freshly prepared 0.9 M aqueous $NaBH_4$ solution were added and the mixture was kept at 0 °C for 3 h. OH-functionalized gold NPs were separated by centrifugation and washed several times with water and toluene. They were stored as stable dispersions in DMF.

Synthesis of $Si(OEt)_3$-functionalized gold NPs

They were prepared by reacting OH-functionalized gold NPs with a slight excess of IPTES with respect to OH groups, using a mixed solvent composed of tetrahydrofuran (THF)/DMF (80:20 by volume). Dibutyltin dilaurate (DBTDL) was used as a catalyst in a 0.5 wt% with respect to IPTES. The reaction was carried out at room temperature for 3 h. NPs were precipitated and washed several times with cyclohexane to remove residual IPTES. They were stored as stable dispersions in DMF.

Film of gold NPs synthesized by a sol–gel process

An aqueous formic acid solution of pH ~4 was added to the dispersion of $Si(OEt)_3$-functionalized gold NPs in DMF, to obtain a molar ratio $H_2O/(OEt) = 1$. The solution was placed onto a glass substrate for 3 days at room temperature, allowing a very slow evaporation of volatiles, leading to a crosslinked film of gold NPs.

Characterization techniques

Fourier-transformed infrared spectra (FTIR)

Fourier-transformed infrared spectra were recorded with a Nicolet 6700 device, in the transmission

mode, including samples in pellets of spectroscopic grade KBr. Dispersions of OH-NPs or $Si(OEt)_3$-NPs in DMF were mixed with KBr and pellets were made after evaporating the solvent. Crosslinked film was crushed to powder and mixed with KBr to make a pellet.

Thermogravimetric analysis

Thermogravimetric analysis was carried out using a Shimadzu TGA-50H device. Sample masses of about 5 mg were placed into alumina pans. Runs were performed at 10 °C/min, from 20 to 950 °C, under N_2 or air.

X-ray diffraction (XRD) spectra

XRD spectra were recorded with an XPert Pro PANalytical device, with the wavelength of CuKα (1.5406 Å). Dispersions of OH-NPs in DMF were casted onto a glass substrate to form a film by evaporation. Crosslinked films were analyzed using the same glass substrate used during the synthetic process.

Transmission electron microscopy (TEM)

Transmission electron microscopy was carried out using a Philips CM-12 device operated at an accelerating voltage of 100 kV. Samples were prepared by dropping 6 μL of the DMF dispersion of gold clusters over a copper grid coated with formvar and a carbon film.

UV–visible spectra

UV–visible spectra were recorded with an Agilent 8453 diode-array spectrophotometer at room temperature. Solutions were placed in a 1 cm × 1 cm × 3 cm quartz cell and solid samples in a special holder. Crosslinked film was supported on a glass microscope slide to record its spectrum. The same glass slide was used as a blank.

Field emission scanning electron microscopy (FESEM)

FESEM Images of surfaces of crosslinked films were obtained with a Zeiss Supra 40 device.

Results and discussion

Small gold NPs coated with MCH were synthesized by the method reported by Tan et al. Reaction of these OH-functionalized NPs with IPTES using DBTDL as a catalyst allows obtaining $Si(OEt)_3$-functionalized gold NPs.

Figure 1 shows FTIR spectra of OH- and $Si(OEt)_3$-functionalized gold NPs. The OH-functionalized NPs exhibit a broad band at about 3,360 cm^{-1} assigned to H-bonded OH groups, a peak at 1,050 cm^{-1} produced by the C–C–O asymmetric stretch of the primary alcohol and characteristic peaks of CH_2 groups at 2,924 and 2,852 cm^{-1}. The characteristic band at 2,550 cm^{-1} due to S–H stretching is not present, meaning that residual MCH was effectively removed by washing and that sulfur atoms are bonded to surface gold atoms.

The FTIR spectrum of $Si(OEt)_3$-functionalized NPs (Fig. 1b) shows characteristic bands of the organic ligands produced by reaction of OH-functionalized gold NPs with IPTES: $–S(CH_2)_6–COO–NH–(CH_2)_3–Si(OCH_2CH_3)_3$. These include the urethane peak at 1,633 cm^{-1}, the Si–O–C asymmetric stretch band at 1,104 cm^{-1}, and the Si-OEt band at 958 cm^{-1}. The absence of an isocyanate peak (2,270 cm^{-1}) means that residual IPTES was completely removed by washing with cyclohexane. However, the conversion of OH to urethane groups was not complete as revealed by the shoulder at 1,050 cm^{-1} and the broad band at about 3,400 cm^{-1} assigned to both residual OH groups and

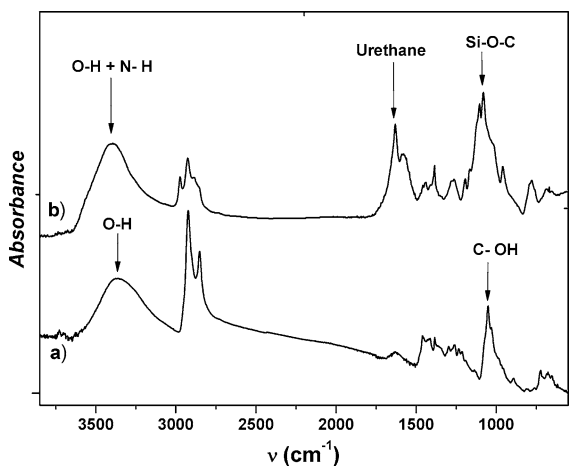

Fig. 1 FTIR spectra of (*a*) OH-functionalized and (*b*) $Si(OEt)_3$-functionalized gold NPs

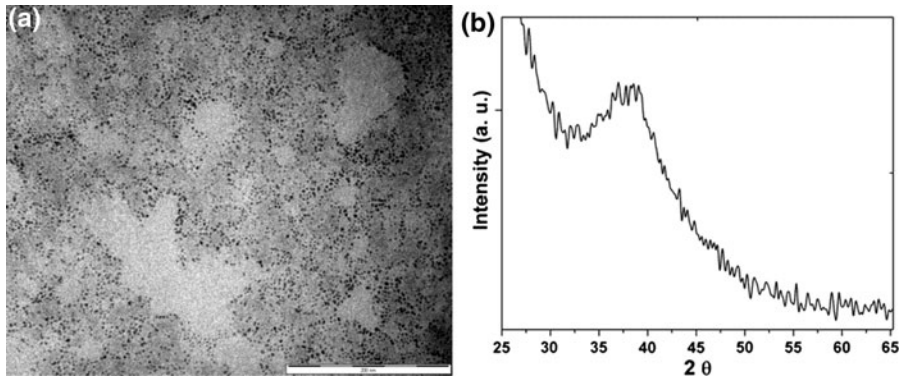

Fig. 2 **a** TEM images of as-synthesized OH-NPs. **b** XRD spectrum of OH-functionalized gold NPs in the range $2\theta = 25°–65°$

generated NH groups. The reaction conditions were established by analyzing the room-temperature reaction of stoichiometric amounts of IPTES and ethanol in a THF/DMF 80:20 solution with different amounts of DBTDL. The reduction in the intensity of the FTIR absorption peak of NCO at 2,276 cm^{-1} was continuously recorded. Using 0.5 wt% DBTDL with respect to IPTES, a complete disappearance of this peak was recorded after about 30-min reaction. A time period of 180 min was selected to carry on the reaction of a slight IPTES excess with the OH-functionalized gold NPs. The partial conversion obtained in our case must be ascribed to the bulky $Si(OEt)_3$ groups present at the end of reacted chains. Once an OH group reacts, it imposes steric restrictions on the access of IPTES to neighboring chains and limits the attainable conversion.

The actual conversion of OH into urethane groups may be estimated from TGA thermograms. The total fractional mass loss gave reproducible values for runs carried out in nitrogen or air for both types of functionalized gold NPs. These values were 18.5 wt% for OH-functionalized gold NPs and 22.9 wt% for $Si(OEt)_3$-functionalized NPs. Using the molar masses of both organic ligands (133.23 and 380.60 Da, respectively) and comparing the expected and actual mass increases, gives a 16.6 % conversion of OH into urethane groups.

TEM images (Fig. 2a) show the presence of particles with sizes lower than about 3 nm. However, a precise determination of the average size could not be made by this technique because of the presence of small clusters of NPs formed during drying over the carbon film (probably induced as a consequence of the strong bonding between ligands). Close proximity of NPs makes difficult to determine a precise characteristic size. However, an estimation of the average size could be made by comparing our experimental results with those obtained by Tan et al. Their OH-functionalized gold NPs, obtained under similar conditions than those used in this study, had an average size of 1.5 nm (determined by HRTEM) and a residual mass percentage (measured by TGA) equal to 81 %. As in our case, the residual mass percentage was 81.5 %; we might estimate that the average size of our NPs was the same as that obtained by Tan et al., within experimental error. An independent estimation of the average size of gold NPs was obtained from their XRD spectrum (Fig. 2b). The most intense characteristic peak of face-centered cubic (*fcc*) gold crystals at $2\theta = 38.25°$ is observed. The average size of gold crystals was estimated from the Scherrer equation (Langford and Wilson 1978):

$$D = k\lambda/B\cos\theta$$

where $k = 0.94$ is the Scherrer constant for spherical crystals with cubic symmetry, $\lambda = 0.154$ nm is the wavelength of the CuKα X-ray radiation, and B is the width at half height of the peak. This gave $D = 1.4$ nm, in excellent agreement with the value estimated from the residual mass fraction.

The UV–visible absorption spectrum of both OH- and $Si(OEt)_3$-functionalized gold NPs in DMF was the same (Fig. 3). A very weak plasmon band centered at about 520 nm is observed which is characteristic of particles with sizes less than 2 nm (Alvarez et al. 1997). This corroborates that the size of NPs was not affected by the reaction with IPTES.

Characterization of films of gold NPs synthesized by a sol–gel process

The films were self-standing, black, and relatively flexible and could be detached from the glass substrate

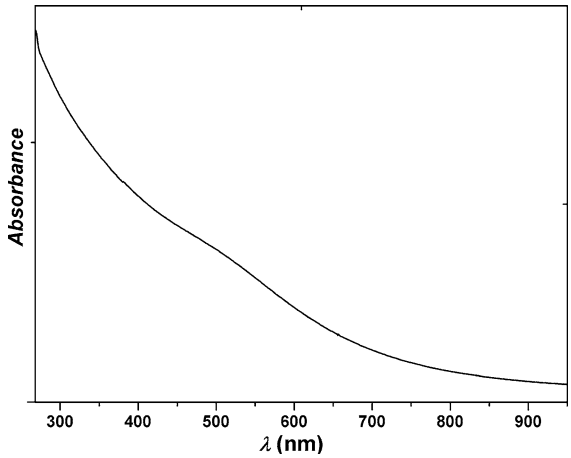

Fig. 3 UV–visible absorption spectrum of OH-functionalized and $Si(OEt)_3$-functionalized gold NPs in DMF

(Fig. 4). The FTIR spectrum of the film is shown in Fig. 5. The strong band at 1,050 cm^{-1} with a shoulder at higher frequencies is assigned to the Si–O–Si antisymmetric stretching (still coupled to the COH band). The Si-OEt band at 958 cm^{-1} disappeared indicating that hydrolysis was complete. The presence of a SiOH band at 904 cm^{-1} evidences that only a partial condensation took place.

The fate of the individual gold NPs in the sol–gel process may be evidenced by the evolution of the plasmon band (Fig. 6). The small increase in intensity and the location of the maximum at about 530 nm reveals that gold NPs were self-assembled but kept their individual size. Ability of the process to preserve size and individuality of gold NPs is important in the efficient transferring of new properties from a colloidal medium to a final device.

FESEM images of the film surface are shown in Fig. 7. The lower magnification (Fig. 7a) evidences the presence of irregular domains containing clusters

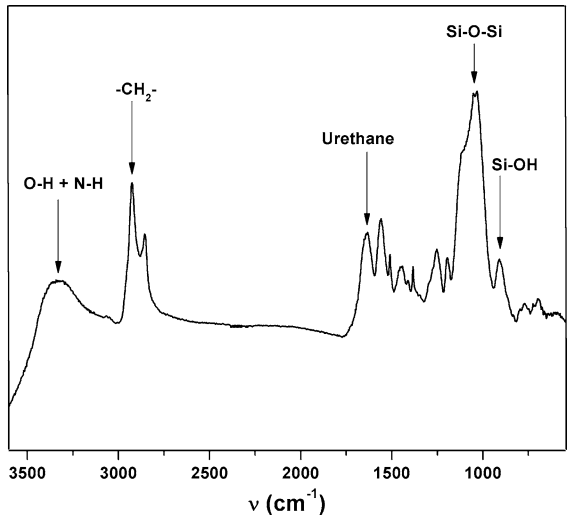

Fig. 5 FTIR spectrum of the film formed by crosslinking the $Si(OEt)_3$-functionalized gold NPs

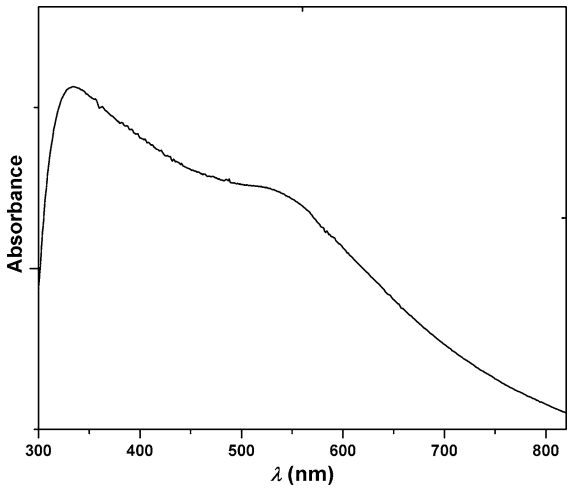

Fig. 6 UV–visible absorption spectrum of the film formed by crosslinking the $Si(OEt)_3$-functionalized gold NPs

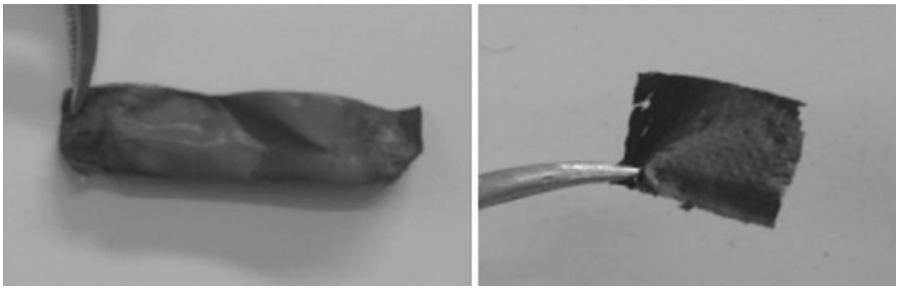

Fig. 4 Photographs of self-standing film formed by crosslinking the $Si(OEt)_3$-functionalized gold NPs by a sol–gel process

of NPs with sizes in the range of 50 nm. The higher magnification (Fig. 7b) focusing on an area that looks smooth in Fig. 7a, shows the presence of clusters of NPs with sizes smaller than 20 nm everywhere in the observation field. It may be inferred that the covalent bonding produced by the sol–gel reaction in the DMF solution led to the generation of clusters with a broad distribution of sizes. These clusters were generated by the covalent bonding of 1.5-nm gold NPs through multiple Si–O–Si bonds. The distribution of sizes arises from a conventional nucleation–growth–coalescence process. At advanced times, solvent evaporation generated the agglomeration of the already existing clusters (those with largest size), forming the irregular domains observed in Fig. 7a. The drying-mediated assembly of clusters is produced by the relatively weak attraction force between nanocrystals that gains importance when the solvent is slowly evaporated (Kinge et al. 2008; Denkov et al. 1993; Kralchevsky and Nagayama 1994; Ohara et al. 1995; Motte et al. 1997; Harfenist et al. 1997; Gelbart et al. 1999; Gómez et al. 1999). At advanced stages of solvent evaporation, the polycondensation process continued producing the interconnection by covalent bonding of clusters with different sizes. Therefore, the final film is composed of interconnected clusters of NPs with a broad distribution of sizes, with those of largest size forming irregular agglomerations dispersed in the whole structure. But what is significant is the fact that the individual 1.5-nm gold NPs kept their individuality inside every crosslinked cluster, as proved by the sensitivity of the nanostructure to an annealing at 100 °C.

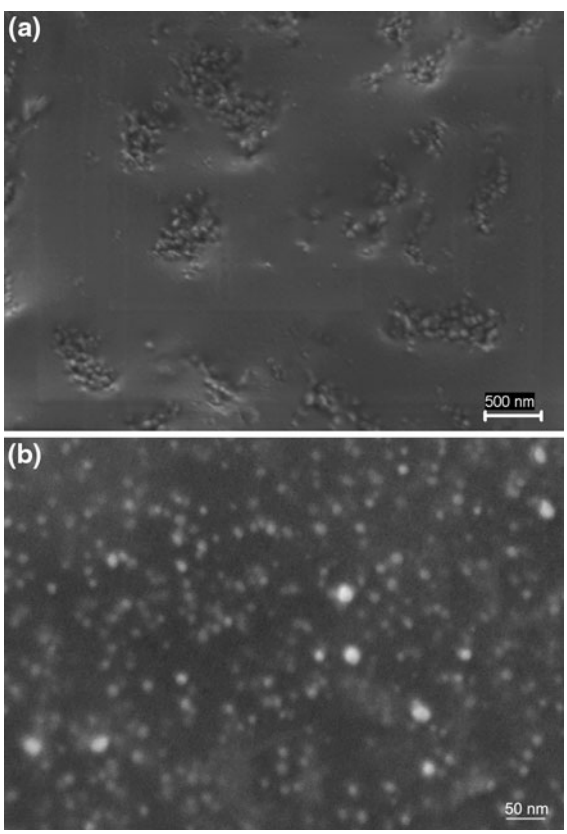

Fig. 7 FESEM images of the film surface synthesized by the sol–gel process at room temperature

Annealing of films at 100 °C

In order to illustrate possible applications of these films, we show structural changes produced by their annealing during 4 h at 100 °C. Due to the low melting point of small gold NPs, it was expected to produce significant changes in the films as a result of this process. It has been already demonstrated that a controlled coalescence of small gold NPs can be produced, both in solution and in solid systems, under specific conditions of thermal treatment. This strategy was proposed for producing monodisperse and highly faceted NPs from solutions of preformed smaller particles (Maye et al. 2000; Maye and Zhong 2000; Zucchi et al. 2008). The coalescence process occurs by thermally induced desorption of organic chains by breaking of the S–Au bond. This is followed by coalescence of the nude gold NPs and partial re-adsorption of the organic chains reforming S–Au bonds. A fraction of the organic groups ends as stable disulfides. This process occurs easily in systems in which very small NPs are in close contact, like in concentrated colloidal dispersions (Maye et al. 2000; Maye and Zhong 2000) or in self-assembled structures stabilized in solid matrices (Zucchi et al. 2008). In our case, films were characterized by regions exhibiting a high concentration of covalently bonded small NPs. This close proximity between particles could enable the coalescence process, to give films characterized by the presence of faceted gold crystals.

After heating, films acquired a reddish coloration indicative of the presence of metallic gold and turned less flexible than the starting films. As evidenced by FESEM images (Fig. 8), the coalescence of 1.5-nm

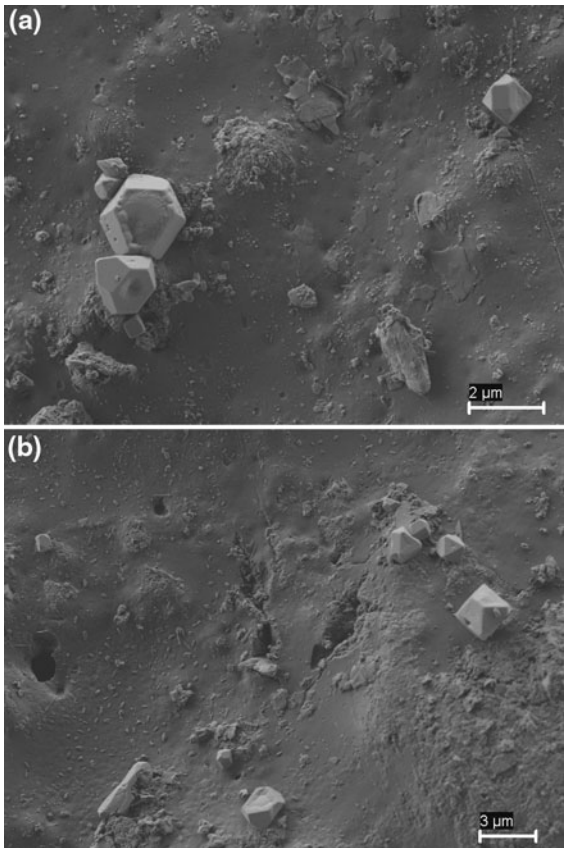

Fig. 8 FESEM images of films annealed at 100 °C for 4 h

gold NPs produced polyhedral gold crystals partially embedded in the film surface and with a broad range of sizes, some of them attaining the micrometer range.

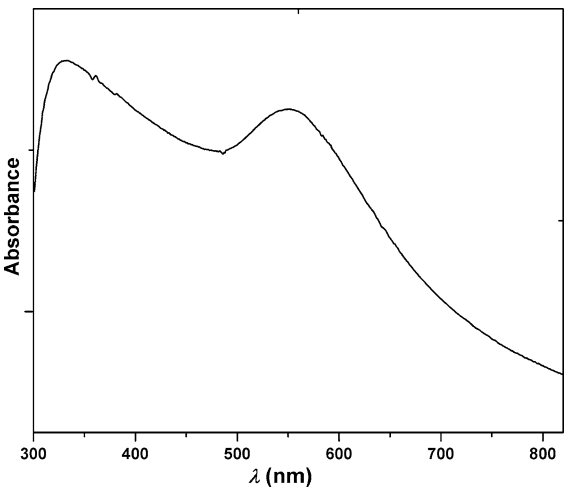

Fig. 9 UV–visible absorption spectrum of the film annealed at 100 °C for 4 h

This might be of interest for the generation of catalytic surfaces or of specific sensors.

The plasmon band was also affected by this annealing process as shown in Fig. 9. A significant increase in its intensity was observed with a shift of the maximum to 555 nm. This is a clear indication of the coalescence of gold clusters produced in the annealing process. The shift and significant change in the intensity of the plasmon band produced by heating to 100 °C may be employed to develop an irreversible sensor of undesirable temperature excursions during the life-time of a specific product.

Conclusions

Self-standing films produced by the covalent bonding of 1.5-nm gold NPs through multiple Si–O–Si bonds, were obtained by a sol–gel process carried out at room temperature. The film structure was composed of crosslinked clusters with sizes up to about 50 nm interconnected through covalent bonds and containing inside the individual 1.5-nm NPs. The drying-mediated assembly produced dispersed irregular domains containing aggregates of large-size clusters.

The possibility of fixing small gold NPs in a crosslinked film opens a variety of potential applications based on the specific properties of small-size particles. As an example, we illustrated the way in which one can take advantage of the low melting temperature of these NPs to generate tiny gold crystals partially embedded at the surface that might be used for the development of specific catalysts or sensors. Besides, the shift and significant change in the intensity of the plasmon band produced by heating to 100 °C may be employed to develop an irreversible sensor of undesirable temperature excursions during the life-time of a specific product.

Acknowledgments Authors acknowledge the financial support of the National Research Council (CONICET, Argentina), the National Agency for the Promotion of Science and Technology (ANPCyT, Argentina), and the University of Mar del Plata.

References

Alvarez MM, Khoury JT, Schaaff TG, Shafigullin MN, Vezmar I, Whetten RL (1997) Optical absorption spectra of nanocrystal gold molecules. J Phys Chem B 101:3706–3712

Baia M, Toderas F, Baia L, Manui D, Astilean S (2009) Multilayer structures of self-assembled gold nanoparticles as a

unique SERS and SEIRA substrate. ChemPhysChem 10: 1106–1111
Buining PA, Humbel BM, Philipse AP, Verkleij AJ (1997) Preparation of functional silane-stabilized gold colloids in the (sub)nanometer size range. Langmuir 13:3921–3926
Denkov ND, Velev OD, Kralchevsky PA, Ivanov IB, Yoshimura H, Nagayama K (1993) Two-dimensional crystallization. Nature 361:26
Eisenberg P, Erra-Balsells R, Ishikawa Y, Lucas JC, Nonami H, Williams RJJ (2002) Silsesquioxanes derived from the bulk polycondensation of [3-(methacryloxy)propyl]trimethoxysilane with concentrated formic acid: evolution of molar mass distributions and fraction of intramolecular cycles. Macromolecules 35:1160–1174
Fan M, Brolo AG (2008) Self-assembled Au nanoparticles as substrates for surface-enhanced vibrational spectroscopy: optimization and electrochemical stability. ChemPhysChem 9:1899–1907
Gelbart WM, Sear RP, Heath JR, Chaney S (1999) Array formation in nano-colloids: theory and experiment in 2D. Faraday Discuss 112:299–307
Ghosh SK, Pal T (2007) Interparticle coupling effect on the surface plasmon resonance of gold nanoparticles: from theory to applications. Chem Rev 107:4797–4862
Gómez ML, Hoppe CE, Zucchi IA, Williams RJJ, Giannotti MI, López-Quintela MA (1999) Hierarchical assemblies of gold nanoparticles at the surface of a film formed by a bridged silsesquioxane containing pendant dodecyl chains. Langmuir 25:1210–1217
Harfenist SA, Wang ZL, Alvarez MM, Vezmar I, Whetten RL (1997) Three-dimensional hexagonal close-packed superlattice of passivated Ag nanocrystals. Adv Mater 9:817–822
Hu M, Yamaguchi K, Okubo T (2005) Self-assembly of water-dispersed gold nanoparticles stabilized by a thiolated glycol derivative. J Nanopart Res 7:187–193
Huo Q, Worden JG (2007) Monofunctional gold nanoparticles: synthesis and applications. J Nanopart Res 9:1013–1025
Kinge S, Crego-Calama M, Reinhoudt DN (2008) Self-assembling nanoparticles at surfaces and interfaces. ChemPhysChem 9:20–42
Ko H, Singamaneni S, Tsukruk VV (2008) Nanostructured surfaces and assemblies as SERS media. Small 4:1576–1599
Kralchevsky PA, Nagayama K (1994) Capillary forces between colloidal particles. Langmuir 10:23–36
Langford JI, Wilson AJC (1978) Scherrer after sixty years: a survey and some new results in the determination of crystallite size. J Appl Cryst 11:102–113
Lim SI, Zhong CJ (2009) Molecularly mediated processing and assembly of nanoparticles: exploring the interparticle interactions and structures. Acc Chem Res 42:798–808
Liz-Marzán LM, Giersig M, Mulvaney P (1996) Synthesis of nanosized gold–silica core–shell particles. Langmuir 12:4329–4335
Maye MM, Zhong CJ (2000) manipulating core–shell reactivities for processing nanoparticle sizes and shapes. J Mater Chem 10:1895–1901
Maye MM, Zheng W, Leibowitz FL, Ly NK, Zhong CJ (2000) Heating-induced evolution of thiolate encapsulated gold nanoparticles: a strategy for size and shape manipulations. langmuir 16:490–497
Motte L, Billoudet F, Thiaudière DA, Naudon A, Pileni MP (1997) Characterization of ordered 3D arrays of Ag_2S nanocrystallites. J Phys III 7:517–527
Ofir Y, Samanta B, Rotello VM (2008) Polymer and biopolymer mediated self-assembly of gold nanoparticles. Chem Soc Rev 37:1814–1825
Ohara PC, Leff DV, Heath JR, Gelbart WM (1995) Crystallization of opals from polydisperse nanoparticles. Phys Rev Lett 75:3466–3469
Prasad BLV, Sorensen CM, Klabunde KJ (2008) Gold nanoparticle superlattices. Chem Soc Rev 37:1871–1883
Rajesh K, Sreedhar B, Radhakrishnan TP (2010) Assembly of gold nanoparticles on a molecular ultrathin film: tuning the surface plasmon resonance. ChemPhysChem 11:1780–1786
Schulzendorf M, Cavelius C, Born P, Murray E, Kraus T (2011) Biphasic synthesis of $Au@SiO_2$ core–shell particles with stepwise ligand exchange. Langmuir 27:727–732
Selvam T, Chiang C-M, Chi KM (2011) Organic-phase synthesis of self-assembled gold nanosheets. J Nanopart Res 13:3275–3286
Sharp KG (1994) A two-component, non-aqueous route to silica gel. J Sol–Gel Sci Technol 1994(2):35–41
Tan H, Zhan T, Fan WY (2006) Direct functionalization of the hydroxyl group of the 6-mercapto-1-hexanol (MCH) ligand attached to gold nanoclusters. J Phys Chem B 110:21690–21693
Wang L, Luo J, Schadt MJ, Zhong CJ (2010) Thin film assemblies of molecularly-linked metal nanoparticles and multifunctional properties. Langmuir 26:618–632
Xiong X, Busnaina A (2008) Direct assembly of nanoparticles for large-scale fabrication of nanodevices and structures. J Nanopart Res 10:947–954
Yamada M, Nishihara H (2004) Large solvent and potential effects on the collective surface plasmon band of gold nanoparticle films. ChemPhysChem 5:555–559
Zucchi IA, Hoppe CE, Galante MJ, Williams RJJ, López-Quintela MA, Matějka L, Slouf M, Pleštil J (2008) Self-assembly of gold nanoparticles as colloidal crystals induced by polymerization of amphiphilic monomers. Macromolecules 41:4895–4903